Progress In Electromagnetics Research C, Vol. 17, 67–78, 2010

THEORY AND APPLICATIONS OF HIGH IMPEDANCE WIRES

M. Shafee

Mentor Graphics Co.
Cairo, Egypt

A. M. Mahmoud

Electrical and Computer Engineering Department
Villanova University, USA

A. M. E. Safwat

Faculty of Engineering
Electronics and Communication Engineering Department
Ain Shams University, Cairo, Egypt

Abstract—This paper presents the theory, properties, types, and applications of high impedance wires (HIWs). The effective permeability of a transmission line that consists of an HIW and a second conductor has a resonating behavior. Consequently, slow-wave and stop-band regions appear in the dispersion relation. In the slow wave regions, a new implementation for dual-mode filter is presented. The proposed filter size is reduced by 33%. In the stop band region, a new application is presented; dual-band balun where the common mode is rejected by the HIW. The novel design has a total area of $4 \times 2.4\,\text{cm}^2$ and exhibits reliable performances at 2.75 GHz with a 40% bandwidth (2.2–3.3 GHz) and at 4.75 GHz with a 15% bandwidth (4.4–5.1 GHz) with an amplitude imbalance less than 1 dB, a return loss better than 13 dB, and phase imbalance less than 5°. Theoretical expectations were confirmed by EM simulations and measurements.

Received 25 September 2010, Accepted 27 October 2010, Scheduled 4 November 2010
Corresponding author: Amr M. E. Safwat (asafwat@ieee.org).

1. INTRODUCTION

Metamaterials with engineered electromagnetic properties have found numerous applications in electromagnetics [1–5]. Among these applications are artificial magnetic surfaces, which are also known as high impedance surfaces (HISs) [6]. HIS consists of electrically small resonant circuits repeated periodically in two dimensions. This configuration prevents the propagation of the wave whose frequency equals to the resonance frequency of the constituent unit cell [7–9].

High impedance wire (HIW) is the one dimensional representation of HIS. It consists of periodic resonant cells in 1D, Hence at resonance; it provides high impedance per unit length [10]. A transmission line with HIW, HIW-TL, emulates a medium that has resonant permeability μ. Before resonance, the slow-wave region allows the realization of compact size microwave devices [11, 12]. At resonance, the permeability switches from positive values to negative values, which creates stop-band. This region can be exploited either to prevent the propagation of unwanted modes [13] or to create left-handed transmission line with the help of complementary (negative permittivity) structures [14].

This paper explains the HIW comprehensively and it introduces two new applications. It is organized as follows: Section 2 discusses the theory and realization of HIWs. Section 3 presents the implementation of a compact size dual-mode filter that operates in the slow-wave region of the HIW-TL. Section 4 presents the implementation of a dual-band HIW balun that operates in the stop-band region of the HIW-TL. Conclusions are drawn in Section 5.

2. THEORY

The behavioral model of HIW-TL consists of identical resonant circuits connected in series as shown in Fig. 1. These resonant circuits can be realized by lumped components or series stubs [10, 11]. If they are present on the signal wire, it is called signal-HIW [11], and if they are present in the ground, it is called ground-HIW [10].

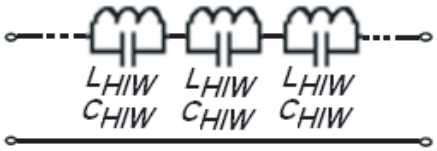

Figure 1. Transmission line with a high impedance wire.

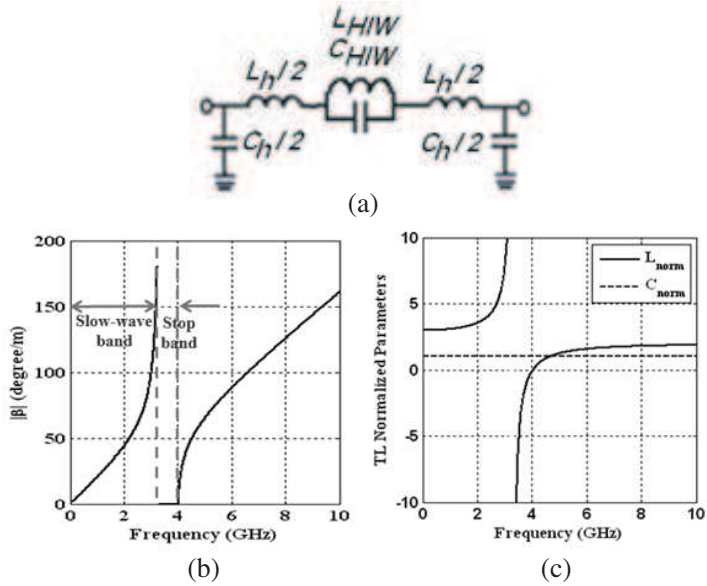

Figure 2. Transmission line with signal-HIW; (a) equivalent model, (b) dispersion curve, (c) normalized inductance and capacitance. Model values: $L_r = 2.76\,\text{nH}$, $C_r = 0.39\,\text{pF}$, $L_{HIW} = 2.7\,\text{nH}$, and $C_{HIW} = 0.86\,\text{pF}$.

The unit cell of a transmission line that has one of its conductors replaced by HIW is shown in Fig. 2(a). The dispersion relation, Bloch impedance, and resonant frequency can be written as follows

$$\beta = \sqrt{j\omega C_h \left(j\omega L_h + \frac{j\omega L_{HIW}}{1 - \frac{\omega^2}{\omega_{HIW}^2}} \right)} \tag{1}$$

$$Z_B = \sqrt{\frac{j\omega L_h}{j\omega C_h + \frac{j\omega L_{HIW}}{1 - \frac{\omega^2}{\omega_{HIW}^2}}}} \tag{2}$$

$$\omega_{HIW} = \sqrt{\frac{1}{L_{HIW} C_{HIW}}} \tag{3}$$

where, C_h and L_h are the host transmission line capacitance and inductance per unit length, and C_{HIW} and L_{HIW} are the equivalent capacitance and inductance of the HIW. Fig. 2(b) shows the dispersion curve of a transmission line with HIW. In order to understand the HIW effect on the effective parameters of the transmission line, two

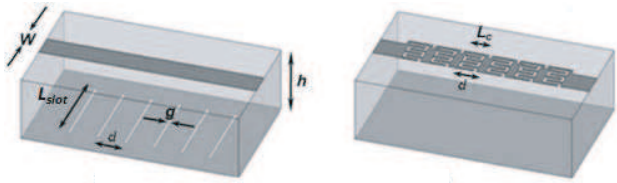

(a) (b)

Figure 3. HIW planar realizations; (a) ground-HIW, (b) signal-HIW.

more quantities are defined; the normalized inductance, L_{norm}, and capacitance, C_{norm}.

$$L_{norm} = \frac{Z_t}{Z_h} \tag{4}$$

$$C_{norm} = \frac{Y_t}{Y_h} \tag{5}$$

where, Z_t and Y_t are the total series impedance and shunt admittance in the unit cell respectively and Z_h and Y_h are the host transmission line series impedance and shunt admittance. Fig. 2(c) shows the effective capacitance and inductance of HIW-TL normalized to the host transmission line capacitance and inductance, L_{norm} has a resonance behavior, while C_{norm} is constant. In terms of material equivalent parameters, before resonance the increase in L_{norm} is equivalent to an increase in the effective permeability, while the effective permittivity is constant. In this band, the HIW-TL behaves as a slow wave structure. After resonance, the normalized inductance has negative values; consequently, the line exhibits negative permeability.

HIW can be realized on the microstrip signal conductor, or ground conductor, or on both. Fig. 3(a) shows a microstrip with slots in the ground plane, which constructs a ground-HIW [10], and Fig. 3(b) shows a signal HIW, where both the inductor and capacitor are patterned on the surface.

3. HIW DUAL-MODE FILTER

Dual-mode filter is obtained by exciting a geometrically symmetrical resonator with orthogonal feed lines. Two degenerate resonant modes are generated. Attaching a small square patch to the loop inner corner couples the degenerate modes, resulting in mode splitting that increases the filter bandwidth and order [15, 16].

The proposed filter replaces the four edges of the resonating loop with signal HIW-TL, as shown in Fig. 4(a). Fig. 4(b) shows the equivalent circuit of the filter. The circuit model consists of two main

parts; the corner patch model, and HIW resonating loop model. The corner patch is modeled as a microstrip right angle bend with width d. The HIW loop consists of 16-HIW cells distributed on the loop four sides.

Two adjacent sides are connected to two orthogonal feed lines using capacitive coupling. These edges and the feed lines are modeled as asymmetric coupled lines. Fig. 5(a) shows HIW unit cells layout and equivalent circuit. Asymmetric coupled line can be modeled by lumped components [17]. Fig. 5(b) shows the circuit model of the coupled lines. It consists of HIW-TL coupled to a conventional TL through coupling capacitance C_m and mutual coupling coefficient K_m, which are tuning parameter. L_{HIW} and C_{HIW} are the HIW inductance and capacitance respectively. L_{h1}, C_{h1}, L_{h2}, and C_{h2} are the inductances and capacitances of the host transmission line and the coupled normal line, respectively. All the model values are listed in the caption of Fig. 5.

The total loop electrical length is 360° at the design frequency (i.e., the loop side electrical-length is 90°). From Fig. 5(c), the HIW cell has 18.35° electrical length at 2.3 GHz, so that the total length of the four cells is 73.4°. The remaining 16.6° are distributed along the two connecting lines (L) and corner-bend capacitors. Fig. 6 shows the effect of the patch size (d) on the resonance frequencies of the two modes. As expected, as d increases, the frequency separation between the two modes increases. Accordingly, to get 100 MHz d was set to 4.5 mm.

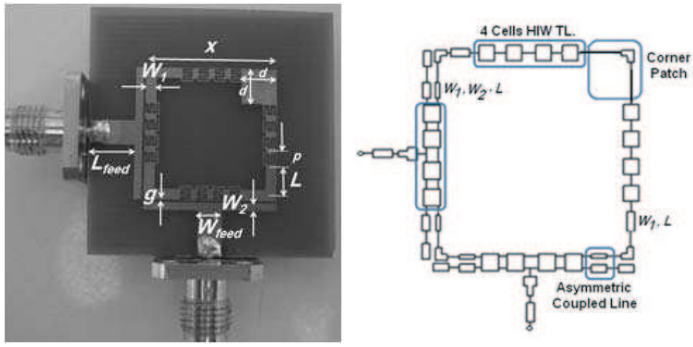

(a) (b)

Figure 4. HIW-DMF, (a) filter prototype, and (b) circuit model. Dimensions: $W_{feed} = 3$ mm, $L_{feed} = 6.4$ mm, $x = 16.4$ mm, $d = 4.5$ mm, $p = 2$ mm, $L = 4.2$ mm, $W_2 = 1$ mm, $g = 0.2$ mm, $W_1 = 1.4$ mm, fingers widths and spaces are 0.2 mm, finger length (L_c) = 1 mm.

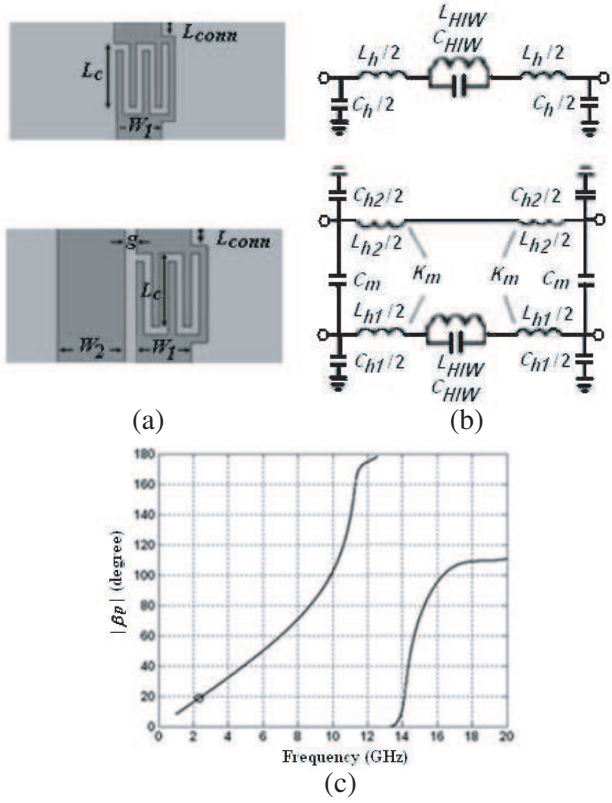

Figure 5. HIW unit cells: (a) single HIW cell, and (b) coupled line cell. Model parameters are $L_{h1} = 0.9\,\text{nH}$, $C_{h1} = 0.16\,\text{pF}$, $L_{h2} = 0.76\,\text{nH}$, $C_{h2} = 0.14\,\text{pF}$, $C_m = 0.1\,\text{pF}$, $K_m = 0.5$, $L_{HIW} = 0.62\,\text{nH}$, $C_{HIW} = 0.12\,\text{pF}$, (c) dispersion characteristics of HIW.

The proposed filter was fabricated on FR4 ($h = 1.6\,\text{mm}$, $r = 4.4$, and $\tan\delta = 0.02$). The comparison between EM, circuit simulations and measurements are shown in Fig. 7. The transmission level is about 3.45 dB; this is due to the large losses of FR4 substrate. Very good agreement between measurements and simulations is achieved. These results show that the filter has two poles at 2.02 and 2.8 GHz, with center frequency at 2.3 GHz. In the proposed implementation, the square loop edge is 16.4 mm, compared to the conventional implementation with 20 mm length; the new structure occupies 67.2% area of the conventional one. This reduction of size was obtained while the inner space of the filter is still free, i.e., there is still room for more reduction [18].

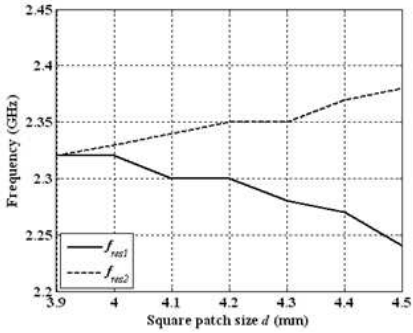

Figure 6. Effect of patch size on mode splitting.

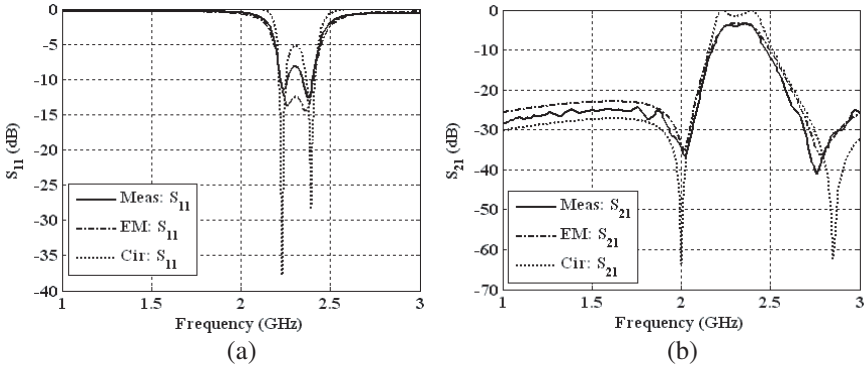

Figure 7. HIW dual-mode filter scattering parameters, (a) S_{11} (dB), (b) S_{21} (dB).

4. HIW DUAL-BAND BALUN

In [13], the HIW was used as the ground plane of microstrip coupled lines to reject the common mode throughout the band of operation, while the top layer was designed as a quarter wave transformer for the matching of the differential mode. Dual stop-band HIW introduces another degree of freedom and permits dual band-stop behavior for the common mode. By achieving this dual band behavior, in addition to maintaining the matching conditions for the differential mode throughout these two bands, a dual band operating balun can be obtained. Fig. 8(a) shows the proposed balun over the dual band HIW-ground. The input port is port 1, the output ports are ports 2 and 3 and port 4 is short-circuited. The input impedance $Z_{in,1}$, as seen at port 1, can be expressed in terms of the input impedances of the

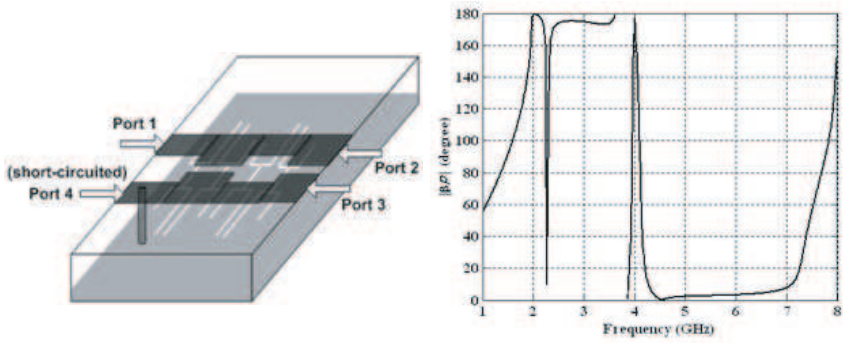

(a) (b)

Figure 8. (a) Proposed structure of the coupled line balun over dual band HIW, 3D prototype. (b) Common mode design dispersion characteristics for the ground-HIW.

differential and common modes as follows [19]

$$Z_{in,1} = \frac{V_1}{I_1} = \frac{4Z_{in,c}Z_{in,d}}{4Z_{in,c} + Z_{in,d}} \tag{6}$$

where, $Z_{in,d}$ and $Z_{in,c}$ are the differential and common mode input impedances respectively. The balun operation is achieved by rejecting the common mode over the two required operating bands, i.e., $Z_{in,c} = \infty$ and achieving matching condition at the input (port 1) and at the differential output (ports 2 and 3). The two chosen center frequencies of the operating bands are 2.8 and 4.8 GHz.

The bottom layer is first designed to reject the common mode throughout the two required bands using the dual band HIW. Using the circuit model shown in [20], an initial design for the dual band HIW was obtained. EM simulations were performed to achieve the best performance with a perfect magnetic conductor symmetry plane, which guarantees the generation of the common mode only. The optimized parameters were the lengths of the ground slots. For $L_1 = 9$ mm and $L_2 = 13$ mm, the dispersion relation is as shown in Fig. 8(b). Two stop-bands appear at 2.2–3.8 GHz and 4.4–7 GHz around 2.2 GHz and 4 GHz, two common-mode pass-bands appear which prevents the realization of ultra wide-band. The number of cells is reduced to minimum to assure compact size balun. For two cells the insertion loss is larger than 10 dB.

The top layer is designed as a low pass filter with a cut-off frequency higher than the upper edge of the second operating band. The source impedance is 50 Ω and the load impedance is 100 Ω (the differential load between ports 2 and 3). The ratio between the load

and source impedance for 0.5 dB ripple Chebyshev filter of even order is approximately 2 to 1, which applies perfectly to this design [21]. A fourth order 0.5 dB ripple low pass filter was considered to keep the top layer's dimensions compatible with the bottom layer. It was implemented as cascaded sections of coupled lines, and as a first order approximation, the inductance and capacitance sections were assumed to be purely inductive and capacitive respectively. For the inductance sections, the lines separation and the line's width were chosen to be 2.5 mm and 3 mm respectively. For a coupled line of these dimensions, the differential mode characteristic impedance $Z_{c,diff}$ and effective permittivity ϵ_{eff} are 90 Ω and 3.1 respectively. Consequently, the inductance per unit length for such a section is 0.53 nH/mm. For the capacitance sections, the lines separation was chosen to be 0.25 mm and the line's width was set to avoid adding discontinuities at the outer edge of the lines between any two subsequent sections. For these dimensions, the capacitance per unit length is 0.1 pF/mm. Consequently, the lengths of the four sections were 3.5 mm, 5 mm, 5 mm and 3.7 mm respectively. Using these dimensions as an initial design, EM optimization was performed using perfect electric-conductors symmetry plane. This simulates only the differential mode. The best results were obtained for dimensions of 3 mm, 6 mm, 3.5 mm and 3.5 mm respectively.

Using the above predetermined dimensions, the balun structure was simulated. The shape of the output feeds was optimized to have minimum return loss while keeping enough separation for the SMA connectors of ports 2 and 3.

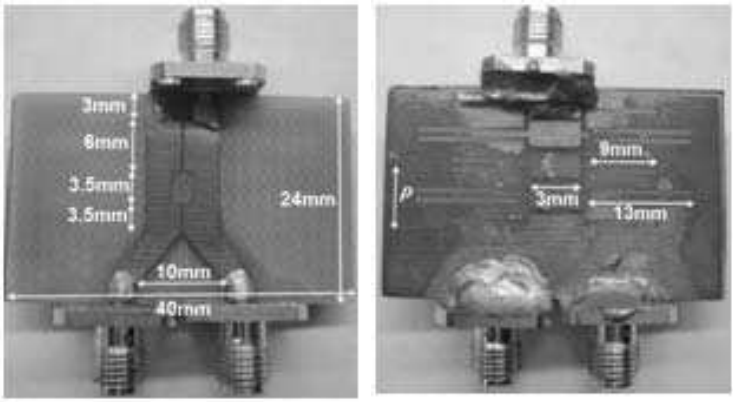

(a) (b)

Figure 9. Dimensions of the fabricated structure, (a) top layer, and (b) bottom layer layout. The pitch $p = 2.7$ mm.

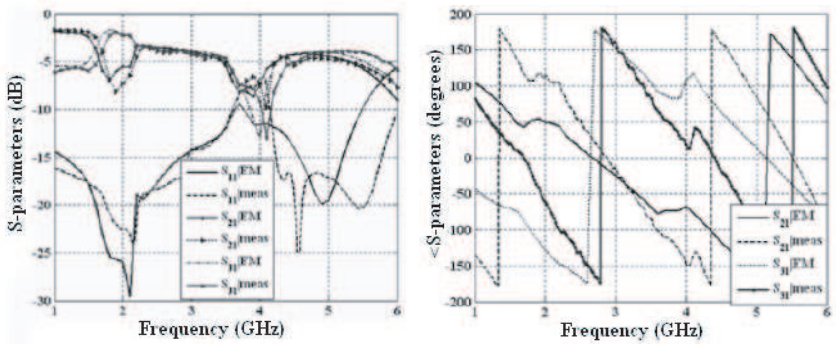

(a) (b)

Figure 10. Measurements and EM simulation results of the dual band HIW-balun, (a) S_{11}, S_{21} and S_{31} magnitude (b) phase of S_{21} and S_{31}.

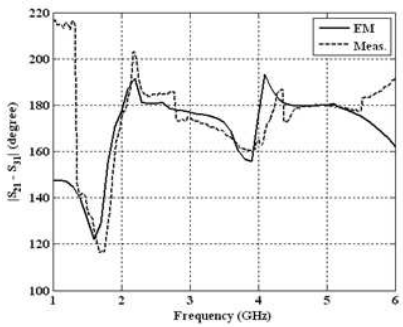

Figure 11. Phase difference between S_{21} and S_{31}.

Figures 9(a) and (b) show the fabricated structure including all the relevant dimensions. EM-simulated and measured S-parameters are inspected in Fig. 10(a). The insertion loss does not exceed 1.5 dB, while the amplitude imbalance between S_{21} and S_{31} does not exceed 1 dB over the two bands of operation. Fig. 10(b) shows the linear variation of the phase of S_{21} and S_{31}, the shift between the simulations and measurements is due to the propagation in the connectors, which are not considered in the EM model. The phase difference between S_{21} and S_{31}, shown in Fig. 11, experiences no more than 5° deviation from the required 180° within the bands.

5. CONCLUSIONS

HIW consists of parallel resonant circuits connected in cascade. When present with another conductor, slow-wave and stop-band regions

appear below the Bragg frequency. This is equivalent to a transmission line that has large (slow-wave) and negative (stop-band) permeability regions. The slow wave phenomenon allows the realization of compact devices. A new implementation for dual mode filter was discussed. The negative permeability or the stop-band permits the rejection of the unwanted frequencies. A dual band balun that operates in this region was presented.

ACKNOWLEDGMENT

This work was supported by the Science and Technology Development Fund (STDF), Egypt under contract number 48.

REFERENCES

1. Chi, P. and T. Itoh, "Miniaturized dual-band directional couplers using composite right/left-handed transmission structures and their applications in beam pattern diversity systems," *IEEE Trans. Microw. Theory Tech.*, Vol. 57, No. 5, 1207–1215, 2009.
2. Engheta, N. and R. W. Ziolkowski, *Metamaterials: Physics and Engineering Explorations*, Wiley-IEEE Press, 2006.
3. Selvanayagam, M. and G. V. Eleftheriades, "Negative-refractive-index transmission lines with expanded unit cells," *IEEE Trans. Antennas and Propagation*, 3592–3596, 2008.
4. Caloz, C., "Dual composite right/left-handed (D-CRLH) transmission line metamaterial," *IEEE Microwave and Wireless Components Letters*, Vol. 16, No. 11, 585–587, 2006.
5. Sindreu, M., A. Vlez, F. Aznar, G. Siso, J. Bonache, and F. Martin, "Applications of open split ring resonators and open complementary split ring resonators to the synthesis of artificial transmission lines and microwave passive components," *IEEE Trans. Microw. Theory Tech.*, Vol. 57, No. 12, 3395–3403, 2009.
6. Sievenpiper, D. F., L. Zhang, R. Broas, N. Alexopolous, and E. Yablonovitvh, "High-impedance electromagnetic surfaces with a forbidden frequency band," *IEEE Trans. Microw. Theory Tech.*, Vol. 47, 2059–2074, 1999.
7. Tran, C.-M., H. Hafdallah-Ouslimani, L. Zhou, and A. C. Priou, "High impedance surfaces based antennas for high data rate communications at 40 GHz," *Progress In Electromagnetics Research C*, Vol. 13, 217–229, 2010.
8. Bao, X. L., G. Ruvio, and M. J. Ammann, "Directional dual-band slot antenna with dual-bandgap high impedance-surface reflector," *Progress In Electromagnetics Research C*, Vol. 9, 1–11, 2009.

9. Abootorabi, S. M., M. Kaboli, S. A. Mirtaheri, and M. S. Abrishamian, "Using high impedance ground plane for improving radiation in monopole antenna and its unusual Reflection phase properties," *PIERS Proceedings*, 197–201, Moscow, Russia, August 18–21, 2009.
10. Safwat, A. M. E., S. A. Tretyakov, and A. V. Raisanen, "High-impedance wire," *IEEE Antennas and Wireless Propagation Letters*, Vol. 6, 631–634, 2007.
11. Shafee, M. A. M., A. M. E. Safwat, and A. H. Morshid, "On the applications on the high impedance wires," *European Microwave Conference (EuMC)*, Roma, Italy, 2009.
12. Shafee, M. A. M. and A. M. E. Safwat, "High impedance wire patch antenna," *European Microwave Conference (EuMC)*, Roma, Italy, 2009.
13. Mahmoud, A. M, M. A Wahby, and A. M. E. Safwat, "Microstrip balun over HIW-ground," *IEEE Microwave and Wireless Components Letters*, Vol. 19, 443–445, 2009.
14. Safwat, A. M. E., "High impedance wire composite right/left handed transmission line," *Microwave and Optical Technology Letters*, Vol. 52, 1390–1393, 2010.
15. Wolff, I., "Microstrip bandpass filter using degenerate modes of a microstrip ring resonator," *Electron. Lett.*, 302–303, 1972.
16. Hong, J. and M. Lancaster, *Microstrip Filters for RF/Microwave Applications*, New York, Wiley, 2001.
17. Caloz, C., A. Sanada, and T. Itoh, "A novel composite right-/left handed coupled-line directional coupler with arbitrary coupling level and broad bandwidth," *IEEE Trans. Microw. Theory Tech.*, Vol. 53, 980–992, 2004.
18. Awida, M., A. Safwat, and H. El-Hennawy, "Miniaturized dual-mode microstrip bandpass filters using meander space-filling curves," *Proceedings of EuMA*, Vol. 2, 187–192, 2006.
19. Salah-Eddin, M. A and A. M. E. Safwat, "Defected-ground coupled microstrip lines and its application in wideband baluns," *IET Microw. Antennas Propag.*, Vol. 1, 893–899, 2007.
20. Abdelaziz, M, A. M. E. Safwat, F. Podevin, and A. Vilcot, "Coplanar waveguide filters based on multibehavior etched-ground stubs," *IEEE Trans. on Components and Packages Technologoes,*, Vol. 32, 816–824, 2009.
21. Pozar, D. M., *Microwave Engineering*, 3rd edition, Wiley, New York, 2003.